Hindawi
Advances in Polymer Technology
Volume 2022, Article ID 1398724, 11 pages
https://doi.org/10.1155/2022/1398724

Research Article

Construction of Dielectric Model of Nonaqueous Reactive Polyurethane Grouting Materials

Meili Meng and Zhanglan Chen

School of Water Conservancy, North China University of Water Resources and Electric Power, Zhengzhou, China

Correspondence should be addressed to Meili Meng; mmlgmx@163.com

Received 12 September 2022; Revised 1 December 2022; Accepted 5 December 2022; Published 20 December 2022

Academic Editor: Milan Mari

In order to reveal the dielectric properties of the nonaqueous reactive polyurethane grouting material, combined with the electron microscope test analysis, it can be seen that the nonaqueous reactive polyurethane material is a porous two-phase body composed of a polyurethane matrix and closed cells. At the microscopic scale, the porous two-phase physical model is established, and the dielectric model of the material is constructed on this basis. In order to verify the dielectric model, 40 groups of nonaqueous reactive polyurethane specimens with different densities were designed and prepared in this paper. The dielectric permittivity was measured by a vector network analyzer (VNA) with an open coaxial probe within the frequency range of 1050 MHz~5010 MHz for the first time, and the dielectric properties and influencing factors were revealed according to the test data. The result shows that the dielectric permittivity of nonaqueous reactive polyurethane materials increases with the increase of density, and decreases slightly with the increase of frequency. Compared with the three models of the Rule of Mixture, Clausius-Mossotti Model and Lichtenecker Model, the calculation accuracy of the Maxwell-Garnett Model is higher, and the calculation results are more consistent with the experimental results of nonaqueous reactive polyurethane grouting materials. The experimental results can be applied to the nondestructive testing of polyurethane grouting materials and provide reference and basis for the quality evaluation of polymer structures.

1. Introduction

As a new type of infrastructure repair and antiseepage grouting material, polyurethane is mostly used in foundation reinforcement, soil densification, filling, antiseepage plugging, and other repair projects [1, 2]. Nondestructive testing equipment can evaluate the pavement quality and grouting effect based on the change of the dielectric properties of the grouting material at different locations in a specific road section [3, 4]. The relative permittivity of a material can characterize its density, and if these values change significantly, defects can be detected [5, 6]. Therefore, in the evaluation of the grouting effect, the determination of the dielectric properties of the polyurethane grouting material will affect the accuracy of the detection. The technique used has limitations in the accurate dielectric properties of solid samples due to errors in the gap between the sample and the open probe [7–10]. More accurate methods for effective measurement of low-loss solid dielectric permittivity in the GHz range are small-band resonator or waveguide-based techniques [11] and broadband coaxial transmission line techniques [12]. However, the testing frequency range of the coaxial probe is wide, the specimen of the measured material is easy to make and process, and the measurement surface only needs to be smooth, which is suitable for the measurement of the dielectric permittivity of solid with a flat surface. Therefore, the use of E5071C network analyzer with terminal open coaxial high temperature probe is more suitable for nondestructive testing of materials.

Polyurethane grouting materials are usually mixed and reacted by two materials of polyol and isocyanate to form a two-phase body with a certain strength, so its dielectric properties can be characterized by a composite dielectric model [13]. The establishment of a comprehensive dielectric

model shows the functional relationship between the relative permittivity of composite materials and the relative permittivity of their components [14, 15].

Polyurethane grouting material is a new type of nonmetallic material widely used in engineering, and most of the previous researches on it focus on engineering performance. Shi et al. studied the change law of compressive strength of polymer-grouting materials at different temperatures and the change law of volume of polymer samples. The results show that the compressive strength of polymer materials increases with the increase of density; at the same density, the compressive strength decreases with the increase of temperature [16]. Zheng et al. prepared polymer-grouting materials with different densities, and systematically studied the bending and compression characteristics of polyurethane polymer-grouting materials with different densities by using three-point bending loading test and unidirectional compression test. The results show that the flexural strength and compressive strength of the polymer grouting material structure increase with the increase of the polymer density as a quadratic function and a linear function, respectively, while the bending deformation capacity decreases with the increase of the density [17].

The current trend in nondestructive testing of civil engineering materials is mainly the detection of defects in concrete and asphalt mix structures, with acoustic methods dominating the field [18, 19]. Beverte et al. conducted a one-year experimental study using a capacitive single-side access sensor to investigate the effects of air temperature, pressure, and relative humidity on the measured permittivity of rigid polyurethane foamed plastics and integral polyurethane of different densities. The results showed that the humidity had the greatest effect on the permittivity [20, 21]. Al-Qadi used the data obtained from 12 different road sections by two GPR systems, and used the air-coupled GPR system to calculate the complex permittivity of hot mix asphalt in the frequency range of 750~1750 MHz [22]. Kim et al. considered 3 water-cement ratios and 4 levels of chloride ion addition in cement mortar samples for dielectric experiments. The results show that the electrical conductivity and dielectric permittivity decrease linearly with the increase of carbonization rate and the decrease of compressive strength, and the coefficient of determination is large [23]. Chen et al. conducted dielectric spectroscopy measurements in the low frequency range ($10^{-2} \sim 10^{6}$ Hz) for different grades of pure asphalt and wax-modified asphalt (WMB) [24]. Yu et al. studied the effects of relative humidity, temperature, and frequency on the dielectric permittivity of asphalt mixtures. The results show that in the temperature range of 30~60°C, the relative permittivity and loss of asphalt mixture increase with the increase of temperature, but the increase rate gradually slows down with the increase of temperature. In the frequency range of 1 kHz~ 1 MHz, the dielectric permittivity of asphalt mixture will decrease with the increase of frequency, and the decreasing rate will increase with the increase of relative humidity [25–27].

Referring to the research ideas on the dielectric properties of asphalt, soil and other related materials, this paper studies the factors affecting the dielectric properties of polyurethane grouting materials. In this paper, the microscopic physical structure is analyzed by electron microscopy experiments, and a porous physical model is established. On this basis, 40 groups of specimens with different densities were prepared by using the self-made grouting mold in the laboratory. In the frequency range of 1050 MHz~5010 MHz, the dielectric permittivity was measured by VNA method using an open coaxial probe. According to the collected test data, the dielectric properties and influencing factors of nonaqueous reactive polyurethane materials were systematically analyzed. Subsequently, the Maxwell-Garnett dielectric model of the nonaqueous polyurethane material was constructed and compared with the other three models. The results demonstrate the validity and high accuracy of the Maxwell-Garnett Model in nonaqueous polyurethane materials.

2. Experiment

2.1. Main Raw Materials. PU is the abbreviation of polyurethane. Polyurethane grouting materials are divided into two types, nonaqueous reactive and water reactive. Nonaqueous reactive polyurethane grouting material (hereinafter referred to as nonaqueous polyurethane material) is a kind of nonaqueous reactive, two-component polyurethane foam material. Different from water-reactive polyurethane materials, nonaqueous polyurethane materials do not require water as a catalyst, so it is only necessary to inject two-component polyurethane raw materials under grouting pressure, and then a chemical reaction occurs, and the volume expands and solidifies to form nonaqueous polyurethane materials [28, 29]. Its main component indexes are shown in Table 1. No water is needed in the reaction process, and the two components are fully mixed and then polymerized to form a solidified body with a certain strength, thereby supporting the overall material. The main reaction in the polymerization process is the gel reaction (as shown in Figure 1), that is, the -NCO group of the isocyanate and the -OH group of the polyol react to form a polyurethane polymer. This reaction process is safe and environmentally friendly, does not emit harmful substances, and the reaction temperature is as high as 175 ± 5°C [30]. The test process is shown in Figure 2.

2.2. Analysis of the Microstructure of the Specimen. As a high molecular polymer foam structure, the performance of nonaqueous polyurethane material is not only related to the density of the polyurethane matrix but also closely related to its cellular structure. The formation of pores is a complex process, which is roughly divided into three stages. (a) Nucleation stage: the gas released by the reaction of the two materials forms a supersaturated solution in the system and then precipitates from the liquid phase to form tiny gas nuclei. This process is also known as a "self-nucleation reaction." (b) Cell growth stage: the gas released by the reaction continuously enters the gas nucleus, and the gas nucleus grows into a bubble and rapidly grows to the estimated volume. Then the bubbles may come into contact with each other to generate and bubble, so that the number of pores in the system is reduced. (c) Cell structure stabilization stage: with the progress of the polymerization reaction, the viscosity of the system increases and gelation occurs, and the size and shape of the cells are fixed to form the final cell structure.

Table 1: Main component indexes of nonaqueous reactive polymer-grouting materials.

Serial number	Project	Polyols	Isocyanates
1	Solid content (%)	>99	>99
2	Density (25°C)/g·cm^{-3}	1.01	1.23
3	Viscosity (25°C)/MPa·s	720 ± 50	350 ± 50
4	-OH/mgKOH·g^{-1}	330 ± 15	——
5	-NCO/wt%	——	21.7 ± 0.5%
6	Moisture content/%	<0.2	0
7	Flash point/°C	>200	>200

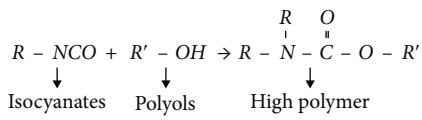

Figure 1: Gel reaction chemical equation.

The macroscopic properties of materials depend on the structure and morphology at the microscopic scale. In view of the porous characteristics of nonaqueous polyurethane materials on the microscopic scale, electron microscopy experiments are required to observe the microstructure of nonaqueous polyurethane specimens. Due to the limited test environment, the electron microscope photo of the reference [31] in this paper deduces the physical model and draws four conclusions.

(1) On the microscopic scale, the nonaqueous polyurethane material is a cellular structure composed of multiple closed-cell cells in close contact, and each cell is an independent and dispersed existence. Therefore, the density of the polyurethane material has a significant relationship with the porosity and the density of the polyurethane matrix. This paper refers to other literatures [32–34] to comprehensively obtain the maximum density of the polyurethane matrix $\rho_s = 1.2\ \mathrm{g/cm^3}$

(2) When the density is small, the shape of the cell is between a circle and a polygon, and the contact surface between each cell is larger. As the density increases, the shape of the pore cells gradually changes from polygonal to elliptical and circular

(3) The cell diameter of the $0.11\ \mathrm{g/cm^3}$ specimen is generally greater than $150\ \mu\mathrm{m}$, and the cell diameter of the $0.40\ \mathrm{g/cm^3}$ specimen is generally less than $220\ \mu\mathrm{m}$. As the density increases, the cell diameter decreases, the contact surface between cells becomes smaller, the free space increases, and the porosity decreases

(4) The matrix between cells is continuous, and as the density increases, the cell wall thickness between adjacent cells also increases

A physical model of its dielectric properties was established through microstructural analysis of electron microscope images, as shown in Figure 3. When constructing its physical model, the nonaqueous polyurethane material can be regarded as a two-phase body composed of a polyurethane matrix and cells. Take a microunit inside the specimen, the volume of the microunit is 1, and the dielectric permittivity value is ε_f. The polyurethane matrix is a continuously distributed medium with a permittivity value of ε_s and a volume of V_s. Cells can be viewed as spheres uniformly distributed in the matrix, with a permittivity value of ε_a and a volume of V_a. According to the effective dielectric theory, ε_f is closely related to ε_s, V_s, ε_a, and V_a.

In order to estimate the porosity of the overall polyurethane specimen, the mass of gas m_a in a unit volume is small relative to the mass m_s of the polyurethane matrix per unit volume and can be ignored

$$m_f = m_s + m_a\,;\ m_a \ll m_s\,;\ m_f \approx m_s. \tag{1}$$

In the equation, the mass of the nonaqueous polyurethane material per unit volume is m_f.

The volume ratio of polyurethane matrix and cell in unit volume of polyurethane material can be expressed as

$$\eta_s = \frac{V_s}{V_f} = \frac{m_s/\rho_s}{m_f/\rho_f} = \frac{\rho_f}{\rho_s}, \tag{2}$$

$$\eta_a = \frac{V_a}{V_f} = \frac{V_f - V_s}{V_f} = 1 - \frac{V_s}{V_f} = 1 - \frac{\rho_f}{\rho_s}. \tag{3}$$

(1) In the equation, V_a and V_s are the volume of cell and polyurethane matrix and V_f is the unit volume of nonaqueous polyurethane specimen, $V_f = 1$

ρ_f, ρ_a, and ρ_s are the densities of the nonaqueous polyurethane material, the cell, and the polyurethane matrix, respectively.

For the cast nonaqueous polyurethane specimen, the density range is controlled within $0.073\ \mathrm{g/cm^3} \le \rho_f \le 0.418\ \mathrm{g/cm^3}$, so the calculated porosity is $93.9\% \ge \eta_a \ge 65.2\%$. This indicates that the material is a high porosity material.

2.3. Dielectric Characteristic Test. Before the experiment, an easily disassembled steel mold was fabricated, as shown in Figure 4(c). The mold is a hollow cylinder with an inner diameter of 70.6 mm, a height of 120 mm, and a wall thickness of 3 mm. The raw materials for the test are shown in Figures 4(a) and 4(b). According to the current standard (GB/T 6343-2009) [35] and (GB/T 12811-1991) [36], the casting, density measurement, and microstructure observation of the test piece were carried out.

In order to facilitate demolding, a lubricating oil film is generally applied on the inner wall of the mold with a brush before pouring. At room temperature (15~20°C), start the grouting equipment and mix the two components into the mold evenly and quickly. After the two materials are mixed, a violent reaction occurs that quickly fills the mold space.

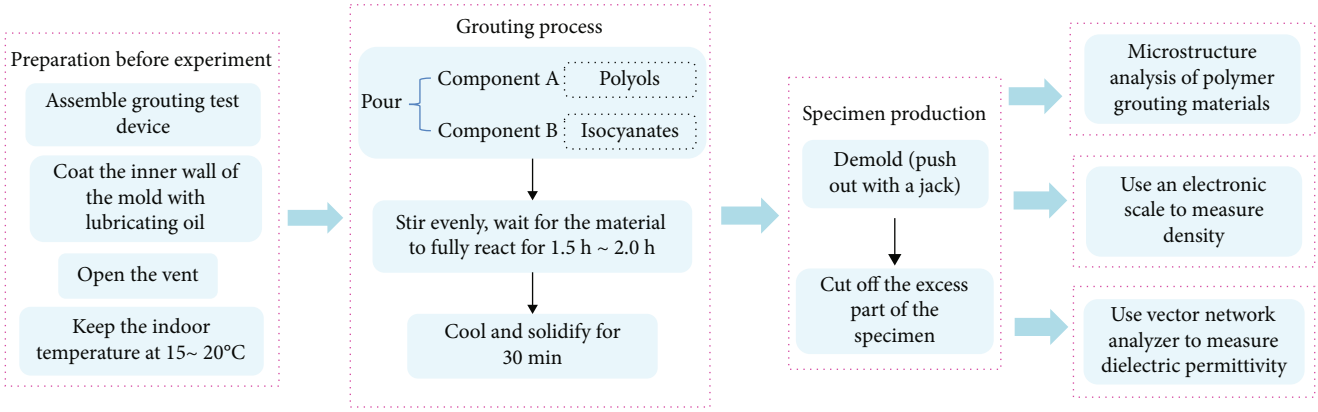

Figure 2: Schematic diagram of the experimental process flow.

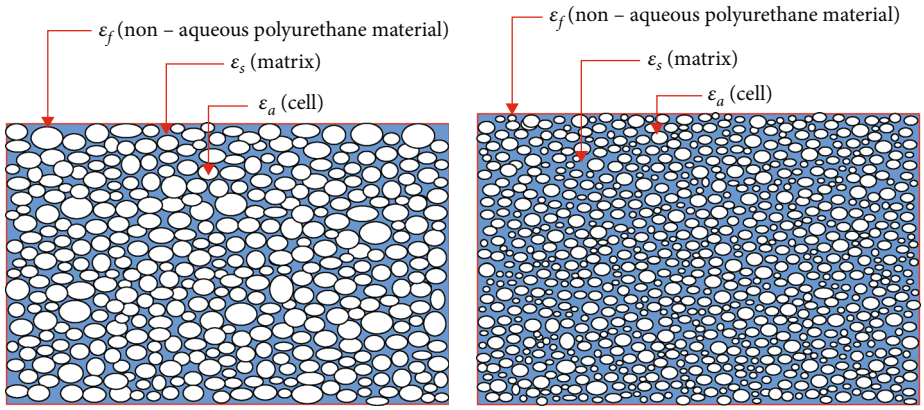

Figure 3: Microphysical model:.(a) Physical model diagram of 0.11 g/cm^3. (b) Physical model diagram of 0.40 g/cm^3.

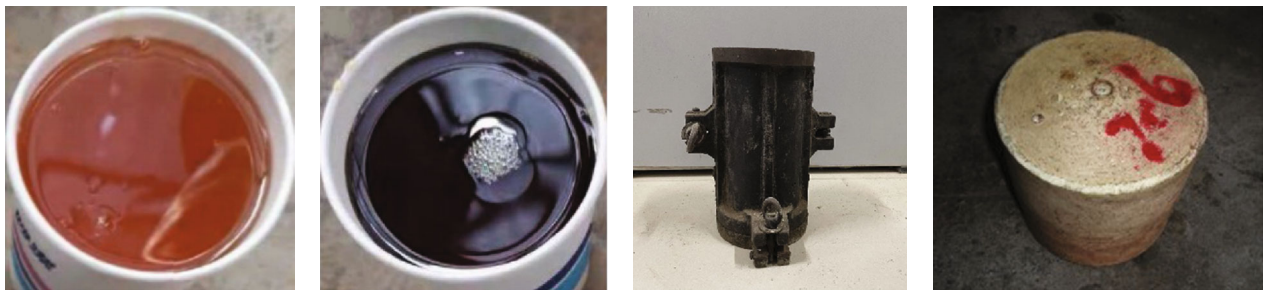

Figure 4: (a) Component A: polyols; (b) component B: isocyanates; (c) mould; (d) polyurethane specimen.

Specimens with different densities can be obtained by controlling the grouting amount, as shown in Figure 4(d). The pouring density range is 0.073 g/cm^3~0.418 g/cm^3. After grouting, wait for the material to fully react and then cool down for 30 minutes before demolding.

Due to the damage or unevenness at both ends of the specimen during the grouting process, it is necessary to cut the specimen to remove defects or redundant parts at the bottom. Determine the final specimen as a cylinder with a diameter of 68 mm and a height of 110 mm, and the error range between each specimen is controlled within ±0.1 mm. A total of 40 specimens with different densities were poured in this test, the weight of each specimen was recorded, its actual density was calculated, and the specimens whose density met the requirements were numbered.

The dielectric permittivity measurement is performed with Agilent's E5071C network analyzer with a terminal open coaxial high temperature probe [37]. The high temperature probe is shown in Figure 4. This probe cannot only measure corrosive chemicals but can also be used to test solids with flat contact surfaces. The testable specimen size is semi-infinite thickness [38].

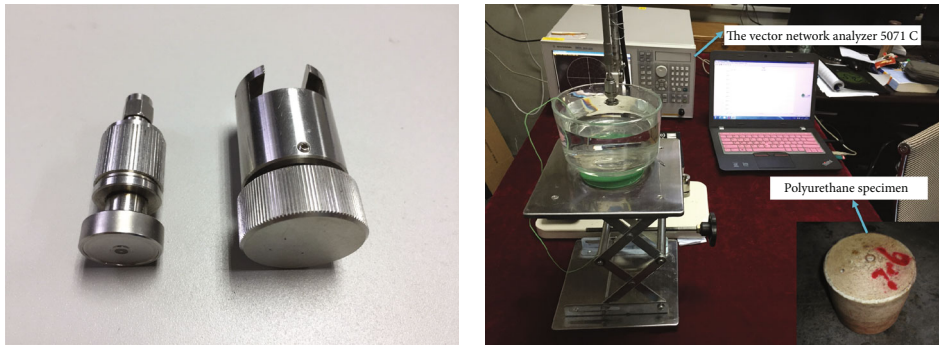

(a) (b)

Figure 5: The dielectric permittivity experiment. (a) High temperature probes. (b) Instrument calibration.

The electromagnetic wave generated by the network analyzer is transmitted to the test piece through the coaxial cable and the probe, and the scattering parameters are measured by measuring the phase and amplitude of the reflected signal at the end of the test piece. The real and imaginary parts of the complex permittivity are then calculated from the scattering parameters using the relevant software and recorded as the final output. The instrument performs an automatic frequency sweep every 50 MHz in the frequency range of 1050 MHz~5010 MHz, and the specific test procedure and results are shown in the reference [39].

Before the test, in order to improve the test accuracy and to eliminate the reflected signal generated by the electromagnetic wave in the discontinuous place, to obtain the relevant parameters, the instrument system must be calibrated using the known medium pure water as the standard (see Figure 5). After calibration, 40 nonaqueous polyurethane specimens with different densities were placed under the probe to measure the dielectric permittivity. During the measurement process, it must be noted that the contact surface should be flat without holes, voids, or air bubbles to avoid errors caused by the incomplete fit between the probe and the object to be measured. In order to improve the measurement accuracy, 10 different measurement points were selected on the measurement surface of each test piece, and the average value was taken as the representative value of the dielectric permittivity of the test piece. During the test, the indoor humidity was 60% and the temperature was 20°C.

3. Construction and Verification of the Dielectric Model

Nonaqueous reactive polyurethane materials are usually considered to be two-phase composite media consisting of matrix and pores. In order to investigate the dielectric properties of this composite as a function of the parameters such as the dielectric permittivity of the single-phase medium and the volume rate occupied by the single-phase medium, the application of the commonly used composite dielectric model to the dielectric properties of nonaqueous reactive polyurethane materials is investigated in relation to the experimental results considering the dielectric properties of the materials.

According to a suitable dielectric model, the dielectric permittivity ε_f can be calculated for any frequency and any material density. It can be seen from the above analysis that in the considered frequency range $1050\,\text{MHz} \le f_n \le 5010$ MHz, the dielectric permittivity value of the gas phase $\varepsilon_a = 1.004$ is selected in this study, and the dielectric permittivity value of the polyurethane matrix is within 4.

3.1. Maxwell-Garnett Model.

$$\varepsilon_f(f_n) = \varepsilon_s(f_n) + \frac{3\eta_a\varepsilon_s(f_n)[\varepsilon_a(f_n) - \varepsilon_s(f_n)]}{\varepsilon_a(f_n) + 2\varepsilon_s(f_n) - \eta_a[\varepsilon_a(f_n) - \varepsilon_s(f_n)]}, \tag{4}$$

where $\varepsilon_s(f_n)$ is the dielectric permittivity of the matrix in the closed cell of the nonaqueous polyurethane material and $\varepsilon_a(f_n)$ is the dielectric permittivity of the gas phase.

The Maxwell-Garnett Model has been successfully applied to predict the dielectric properties of mixtures with low volume filling ratios ($v_a \le 1$) [40]. However, as the volume fraction of the matrix phase increases, the Maxwell-Garnett Model estimates begin to deviate, which occurs especially in the case of high dielectric permittivities between the matrices that make up the mixture.

3.2. The Rule of Mixture. According to the porous and closed-cell microstructure characteristics of the nonaqueous polyurethane material, it is regarded as a two-phase composite material composed of a polyurethane matrix and a gas phase, and the nonaqueous polyurethane specimen is in a dry and anhydrous state in the test. From the parallel model, the two components in the material are considered to be in parallel mode when the particle size is similar to the thickness of the sample [41]. It is assumed that the dielectric permittivity at each single frequency is the volume-weighted average of the dielectric permittivity of each phase.

$$\varepsilon_f(f_n) = \varepsilon_s(f_n)V_s + \varepsilon_a(f_n)V_a, \tag{5}$$

where $V_a \longrightarrow 0$, $\varepsilon_f(f_n) \longrightarrow \varepsilon_s(f_n)$, $V_s \longrightarrow 0$, and $\varepsilon_f(f_n) \longrightarrow \varepsilon_a(f_n)$.

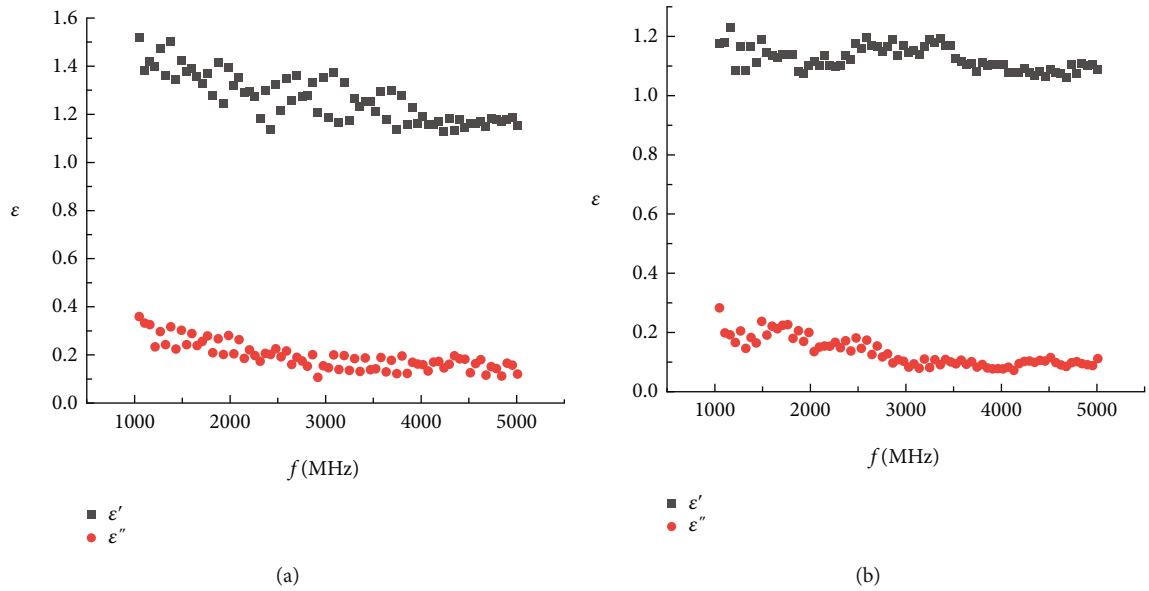

Figure 6: Measured dielectric spectra of (a) sample 1 and (b) sample 30.

From Equations (2), (3), and (5),

$$\varepsilon_f(f_n) = \varepsilon_s(f_n)\eta_s + \varepsilon_a(f_n)\eta_a. \tag{6}$$

3.3. Clausius-Mossotti Model. In the Clausius-Mossotti Model, the polyurethane matrix is regarded as a continuous and homogeneous medium, and closed-cell bubbles are dispersed spheres embedded in the continuous matrix. The polarization is not affected by the applied electric field, and the charge fills the interface between the closed cells and the polyurethane matrix and generates an internal electric field. Then, the effective dielectric permittivity of the two-phase composite can be expressed as

$$\frac{\varepsilon_f(f_n) - \varepsilon_a(f_n)}{\varepsilon_f(f_n) + 2\varepsilon_a(f_n)} = \eta_s \frac{\varepsilon_s(f_n) - \varepsilon_a(f_n)}{\varepsilon_s(f_n) + 2\varepsilon_a(f_n)}, \tag{7}$$

where $\eta_s \longrightarrow 1$, $\varepsilon_f(f_n) \longrightarrow \varepsilon_s(f_n)$, $\eta_s \longrightarrow 0$, and $\varepsilon_f(f_n) \longrightarrow \varepsilon_a(f_n)$.

However, this model is suitable for high frequencies. Or when polar molecules form dilute solutions in nonpolar solvents, the Clausius-Mossotti Model predicts well.

3.4. Lichtenecker Model. Polyurethane materials are considered to be two-phase mixtures of polyurethane matrix and cellular combinations. To calculate the effective dielectric permittivity, the Lichtenecker Model can be expressed as

$$\varepsilon_f = \prod_{k=1}^{K} \varepsilon_k{}^{v_k}. \tag{8}$$

When the number of components $K = 2$, take the natural logarithm on both sides of the equation.

$$\varepsilon_f(f_n) = \varepsilon_s(f_n)^{\eta_s}\varepsilon_a(f_n)^{\eta_a}. \tag{9}$$

It can be seen from the above four models that if $\eta_s \longrightarrow 1$, that is, when $\eta_a = 0$, then $\varepsilon_f(f_n)$ is only related to the permittivity and density of the material, and the permittivity values calculated by each model are equal. Therefore, the influence of porosity must be considered when calculating the dielectric permittivity of nonaqueous polyurethane materials. Because the nonaqueous polyurethane material is a two-phase mixture, its porosity is very high ($93.9\% \geq \eta_a \geq 65.2\%$), and the dielectric permittivity of the gas phase $\varepsilon_a = 1.004$, so the dielectric permittivity of the nonaqueous polyurethane is very low (≤2). For example, the density range of the nonaqueous polyurethane specimen measured in this test is $0.073\,\text{g/cm}^3 \leq \rho_f \leq 0.418\,\text{g/cm}^3$, and the dielectric permittivity value is within the range of $1.109 \leq \varepsilon_f \leq 1.769$

4. Results and Discussion

This test instrument performs automatic frequency sweep measurements every 50 MHz in the frequency range of 1050 MHz~5010 MHz. The measured data of specimen 1 ($\rho = 0.418\,\text{g/cm}^3$) and specimen 30 ($\rho = 0.31\,\text{g/cm}^3$) were randomly selected to plot the dielectric spectra (see Figure 6). From the measured data points in Figure 6, it can be seen that the data results of the coaxial probe method of measurement have a high dispersion, while the selection of measurement points and the fit of the measurement also have a large impact on the results, thus producing errors in the test results. However, as can be seen in Figure 6, both the real and imaginary parts of the dielectric permittivity decrease with increasing frequency. This may be due to the fact that the interfacial polarization and space charge polarization processes gradually fail to keep up with the frequency change during the gradual increase of frequency, which leads to the decrease of the dielectric constant.

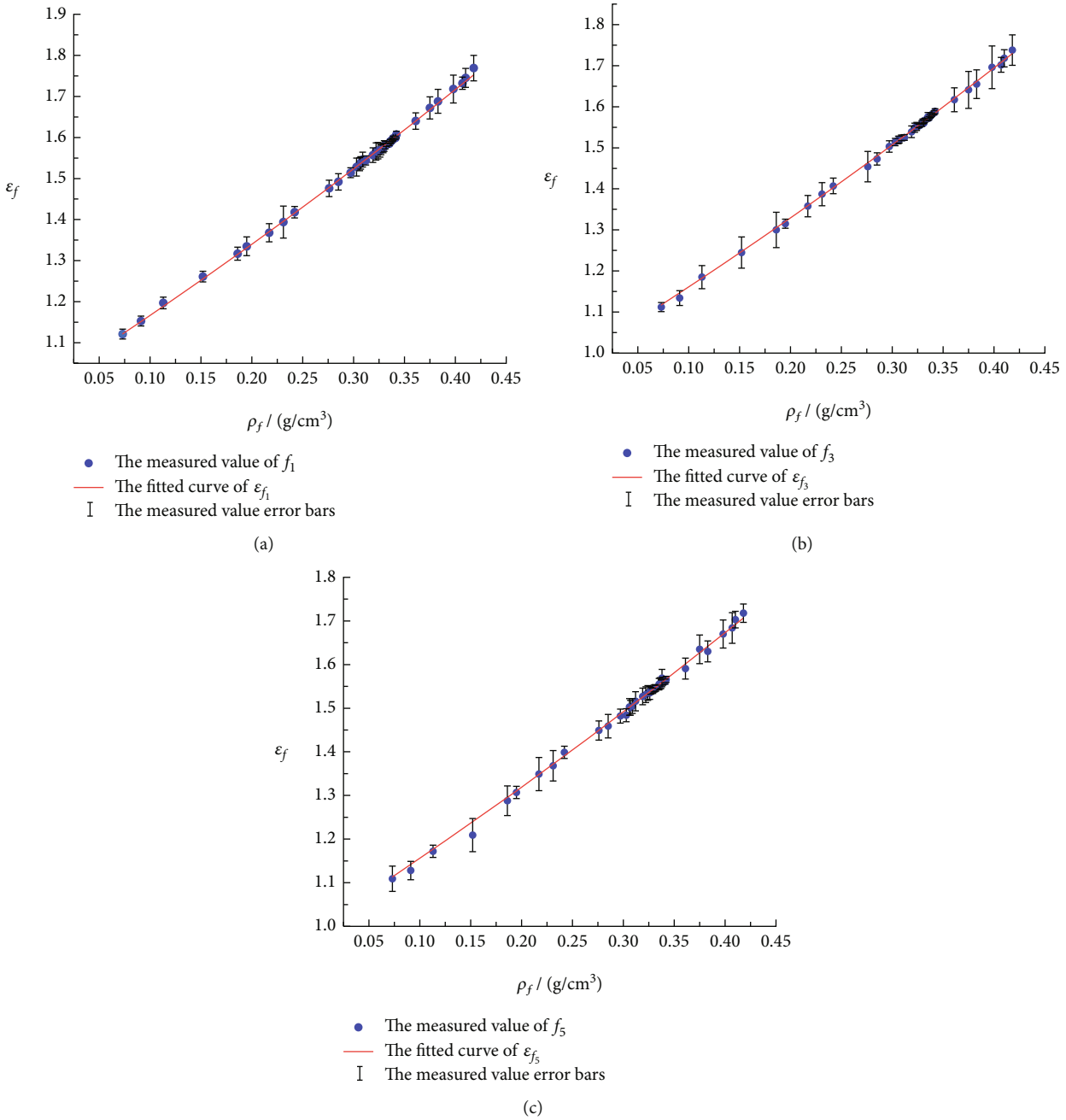

FIGURE 7: Relationship between dielectric permittivity and density at three frequencies. (a) $f_1 = 1050$ MHz; (b) $f_3 = 3030$ MHz; (c) $f_5 = 5010$ MHz.

4.1. Relationship between ε_f and ρ_f. In this test, an automatic frequency sweep measurement is performed at 50 MHz intervals in the frequency range of 1050 MHz~5010 MHz, and the data at three frequencies are selected as representative for analysis: $f_1 = 1050$ MHz, $f_3 = 3030$ MHz, and $f_5 = 5010$ MHz. Analysis of the test data found that the dielectric permittivity increased with the increase of the density of the specimen, as shown in Figure 7. At other frequencies, the trend line for experimental data $\varepsilon_f = \varepsilon_f(\rho_f)$ is similar.

It can be seen from Figure 7 that the density range of the nonaqueous polyurethane specimen measured by the test is $0.073\ \text{g/cm}^3 \le \rho_f \le 0.418\ \text{g/cm}^3$, and the relationship between the dielectric permittivity and the density is positively correlated. In the frequency range of 1050 MHz~5010 MHz, the dielectric permittivity decreases slightly with the increase of frequency.

$\varepsilon_f = \varepsilon_f(\rho_f)$ is slightly nonlinear and can be well approximated by the least squares method of second-order polynomials

$$\varepsilon_{f_1} = 1.004 + 1.5765\rho_f + 0.5115{\rho_f}^2, f_1 = 1050\ \text{MHz}, \quad (10)$$

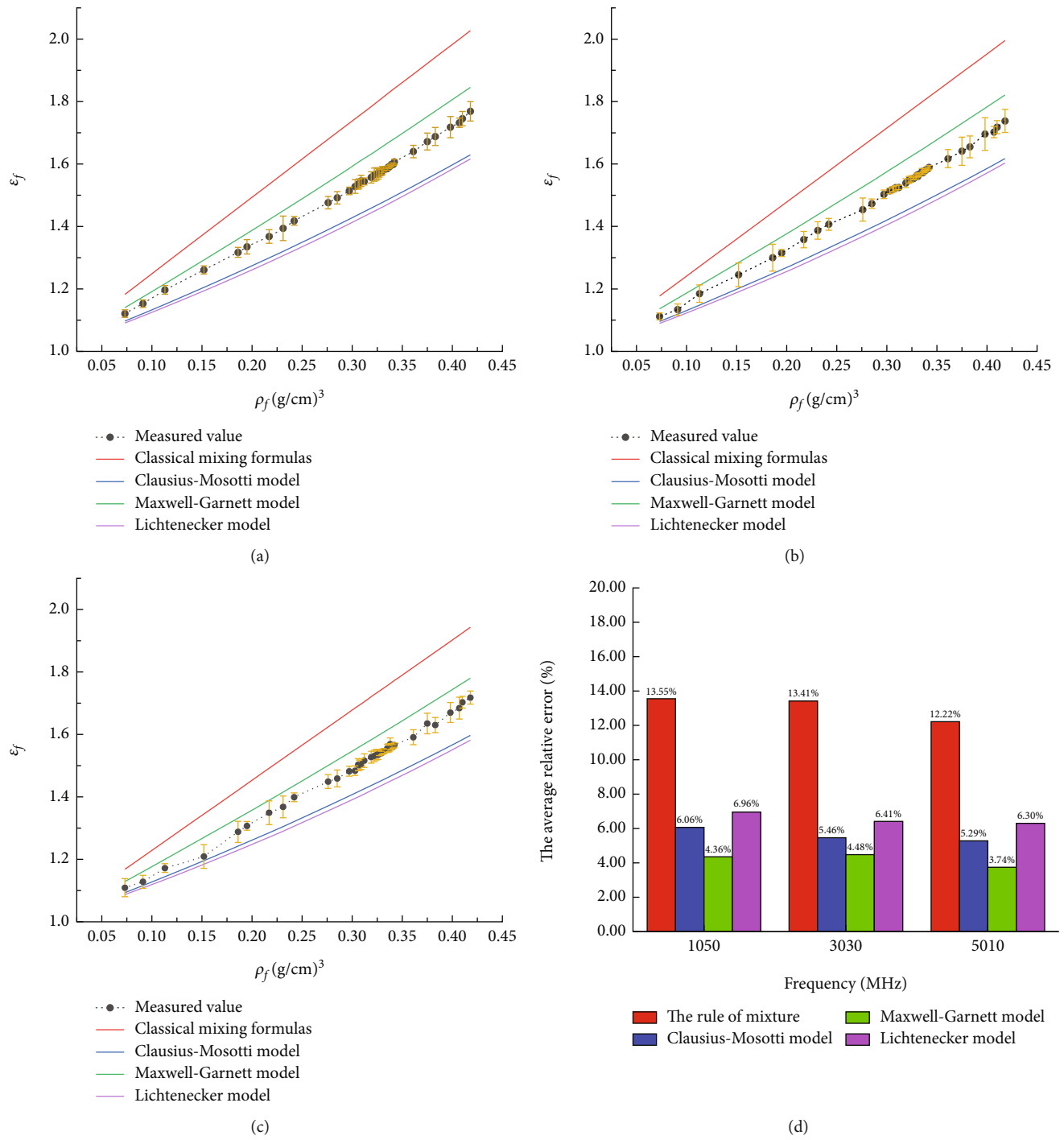

FIGURE 8: Model comparison and error analysis diagram. (a) $f = 1050$ MHz, (b) $f = 3030$ MHz, (c) $f = 5010$ MHz; (d) average relative error of different models at different frequencies.

$$R^2 = 0.995, \tag{11}$$

$$\varepsilon_{f_3} = 1.003 + 1.5318\rho_f + 0.4935{\rho_f}^2, f_3 = 3030\ \text{MHz}, \tag{12}$$

$$R^2 = 0.995, \tag{13}$$

$$\varepsilon_{f_5} = 1.002 + 1.4879\rho_f + 0.4723{\rho_f}^2, f_5 = 5010\ \text{MHz}, \tag{14}$$

$$R^2 = 0.995, \tag{15}$$

Among them, R^2 is the coefficient of determination, and $R^2 = 0.995$ indicates that the fitting degree is very good.

From the fitting relationship between the permittivity and density of Equations (10), (12), and (14), it can be known that

(1) When the density of the nonaqueous polyurethane specimen is $\rho_f \longrightarrow \rho_s = 1.2\ \text{g/cm}^3$, the dielectric permittivity of the polyurethane matrix can be

calculated. When $f = 1050$ MHz, $\varepsilon_{f_1} = \varepsilon_s = 3.632$; when $f = 3030$ MHz, $\varepsilon_{f_3} = \varepsilon_s = 3.5519$; when $f = 5010$ MHz, $\varepsilon_{f_5} = \varepsilon_s = 3.468$. In the frequency range of 1050 MHz~5010 MHz, the dielectric permittivity value of the polyurethane matrix determined by the experiment is within 4, and it decreases slightly with the increase of frequency

(2) When the density of the nonaqueous polyurethane specimen is $\rho_f \to 0$, the dielectric permittivity of the gas phase can be calculated. When $f = 1050$ MHz, $\varepsilon_{f_1} = \varepsilon_a = 1.004$; when $f = 3030$ MHz, $\varepsilon_{f_3} = \varepsilon_a = 1.0031$; when $f = 5010$ MHz, $\varepsilon_{f_5} = \varepsilon_a = 1.0024$. In the considered frequency range $1050\text{ MHz} \le f_n \le 5010$ MHz, the limit value of the gas phase dielectric permittivity value determined by this test is $1.004 \ge \varepsilon_a \ge 1.0024$. This is consistent with the dielectric permittivity value ε_a of most gases in the range of 1.00006~1.01, such as the dielectric permittivity of helium $\varepsilon_{\text{He}} = 1.0000605$, the dielectric permittivity of dry air $\varepsilon_{\text{dry air}} = 1.000536$, and the dielectric permittivity of methyl bromide $\varepsilon_{\text{CH}_3\text{Br}} = 1.01028$ [42, 43]

Considering that the reference frequency range of 1050 MHz~5010 MHz is lower than the infrared radiation frequency of 300 GHz, it is assumed that the dielectric permittivity of the gas phase is constant for the above frequencies. Therefore, the dielectric permittivity value $\varepsilon_a = 1.004$ of the gas phase is selected for further calculation in this study. This conclusion also lays the foundation for the establishment of the dielectric model of the nonaqueous polyurethane material in the following.

4.2. ε_f Calculated by Different Dielectric Models. The four models established by the above analysis assume that the maximum density of the polyurethane matrix $\rho_s = 1.2$ g/cm^3. According to Equations (2) and (3), η_s and η_a with different densities were calculated and substituted into each model to obtain the calculated permittivity values of models with different densities at different frequencies, and then compared and analyzed with the measured permittivity values. As a result, as shown in Figure 8, the dielectric permittivity of the nonaqueous polyurethane material has a strong dependence on the density. The higher the density, the higher the dielectric permittivity. It also has a certain frequency dependence, with the dielectric permittivity decreasing slightly as the frequency increases.

The model comparison analysis chart and relative error chart under the three frequencies in Figure 8 all show that

(1) All experimental data points lie between the boundaries determined by the mixing law (top) and the Lichtenecker Model (bottom)

(2) The dielectric permittivity value calculated by the mixing law is the largest, and the average error of the calculation exceeds 12%. This is because the mixing law simply adds the two-phase substances, and does not consider that part of the gas in the overall polymer is produced by the mixing reaction of the two materials, so $\varepsilon_f(f_n)$ is not just a simple addition of the two phases

(3) The calculation results of the Clausius-Mossotti Model and the Lichtenecker Model are very close, and the average relative error of calculation is about 5%~7%, but the calculation result of the Lichtenecker Model is always lower than that of the Clausius-Mossotti Model. This is because in the Lichtenecker Model, although the dielectric permittivity of the two-phase medium increases exponentially with the porosity, the porosity of the material does not exceed 1 at low densities ($0.073\text{ g/cm}^3 \le \rho_f \le 0.418\text{ g/cm}^3$). Therefore, the value of the dielectric permittivity calculated with the Lichtenecker Model increases minimally at low densities

(4) The average relative error of the Maxwell-Garnett Model is the smallest, all around 4%. Therefore, compared with the mixing law, Clausius-Mossotti Model and Lichtenecker Model, the Maxwell-Garnett Model has higher prediction accuracy in calculating the dielectric permittivity of nonaqueous polyurethane materials

5. Conclusion

In this study, combined with previous experience, the first attempt was made to study the dielectric permittivity of nonaqueous polyurethane materials at different densities and frequencies using a vector network analyzer with an open coaxial probe in the frequency range of 1050 MHz to 5010 MHz. Three conclusions are drawn from the research and analysis, which can provide reference for the evaluation of grouting effect of nonaqueous polyurethane materials by nondestructive testing methods.

(1) The macroscopic properties of a material depend on its structure at the microscopic scale. As polymeric materials are closed-cell and porous, with the increase of density, the shape of pore bubbles gradually changes from polygon to oval and round, and the diameter decreases. The contact surface between the pore bubble is small, the free space is large (matrix increase), and the porosity is also decreasing

(2) In this experiment, the dielectric permittivity values of nonaqueous reactive polyurethane grouting material at different frequencies and densities of 1050 MHz~5010 MHz were tested, and the regression analysis was made. The second order multinomial fitting relation between dielectric permittivity and density at different frequencies is established, and the mechanism of dielectric permittivity increasing with density is revealed. And the dielectric permittivity decreased slightly with the increase of frequency

(3) The monolithic nonaqueous polyurethane specimen was considered as a "polymer-gas phase" heterogeneous medium, and the Maxwell-Garnett Model

was compared with the other three models. The results show that the Maxwell-Garnett Model is more suitable for predicting the dielectric properties of nonaqueous polyurethane materials, and the average error between the calculated value and the measured value is less than 5%, which is significantly higher than the other three prediction models. In the future, the Maxwell-Garnett Model can be used to estimate the dielectric permittivity of nonaqueous reactive polyurethane materials

Due to the limitation of experimental methods, the research on the dielectric permittivity of nonaqueous polyurethane materials in this paper has not considered the influence of the wet state, and further research is needed in the later stage.

Data Availability

All data are available from the corresponding author.

Conflicts of Interest

The authors declare that they have no conflicts of interest.

Acknowledgments

This research is supported by the National Natural Science Foundation of China (Nos. 51608197 and 51679091) and the Key Research Projects of Henan Higher Education Institutions (No. 23B570001).

References

[1] M. L. Xu, X. F. He, J. F. Li, D. B. Lv, H. L. Huang, and X. X. Cao, "Research on application of polyurethane grouting material for mining," *Materials Reports*, vol. 28, no. 17, pp. 96–100, 2014.

[2] C. C. Guo, *Study on Non-water Reacted Polymer Curtain Grouting for Seepage Control of Dykes and Dams*, Dalian University of Technology, Dalian, 2012.

[3] H. Liu and M. Sato, "In situ measurement of pavement thickness and dielectric permittivity by GPR using an antenna array," *NDT & E International*, vol. 64, pp. 65–71, 2014.

[4] M. A. Rasol, V. Pérez-Gracia, F. M. Fernandes, J. C. Pais, M. Solla, and C. Santos, "NDT assessment of rigid pavement damages with ground penetrating radar: laboratory and field tests," *International Journal of Pavement Engineering*, vol. 23, no. 3, pp. 900–915, 2022.

[5] X. T. Xiao, *A Study on Non-destructive Testing of Concrete Based on Ground Penetrating Radar*, South China University of Technology, Guangzhou, 2013.

[6] D. H. Chen, F. Hong, W. J. Zhou, and P. Ying, "Estimating the hotmix asphalt air voids from ground penetrating radar," *NDT & E International*, vol. 68, pp. 120–127, 2014.

[7] A. Fallahi, S. Hashemizadeh, and N. Kuster, "Dielectric spectroscopy of high permittivity thin solids using open-ended coaxial probes," in *2022 16th European Conference on Antennas and Propagation (EuCAP)*, pp. 1–4, Madrid, Spain, 2022.

[8] J. Grant, R. Clarke, G. Symm, and N. M. Spyrou, "A critical study of the open-ended coaxial line sensor technique for RF and microwave complex permittivity measurements," *Journal of Physics E: Scientific Instruments*, vol. 22, no. 9, pp. 757–770, 1989.

[9] G. Jiang, W. Wong, E. Raskovich, W. Clark, W. Hines, and J. Sanny, "Open-ended coaxial-line technique for the measurement of the microwave dielectric constant for low-loss solids and liquids," *Review of Scientific Instruments*, vol. 64, no. 6, pp. 1614–1621, 1993.

[10] P. M. Meaney, A. P. Gregory, J. Seppälä, and T. Lahtinen, "Open-ended coaxial dielectric probe effective penetration depth determination," *IEEE Transactions on Microwave Theory and Techniques*, vol. 64, no. 3, pp. 915–923, 2016.

[11] U. Kaatze, "Techniques for measuring the microwave dielectric properties of materials," *Metrologia*, vol. 47, no. 2, pp. S91–S113, 2010.

[12] U. C. Hasar, "Unique retrieval of complex permittivity of low-loss dielectric materials from transmission-only measurements," *IEEE Geoscience and Remote Sensing Letters*, vol. 8, no. 3, pp. 562–564, 2010.

[13] D. Y. Yang, *Research on Highway Asphalt Pavement Inner Disease Quick Maintenance of High Polymer Grouting and Application*, Engineering of Wuhan University, Wuhan, 2015.

[14] Y. Zhai, B. Zhang, F. Wang, Y. Zhong, and X. Li, "Composite dielectric model of asphalt mixtures considering mineral aggregate gradation," *Journal of Materials in Civil Engineering*, vol. 31, no. 6, p. 04019091, 2019.

[15] M. L. Meng and F. M. Wang, "Theoretical analyses and experimental research on a cement concrete dielectric model," *Journal of Materials in Civil Engineering*, vol. 25, no. 12, pp. 1959–1963, 2013.

[16] M. S. Shi, F. M. Wang, and J. Luo, "Compressive strength of polymer grouting material at different temperatures," *Journal of Wuhan University of Technology*, vol. 25, no. 6, pp. 962–965, 2010.

[17] X. G. Zheng, S. M. Li, Y. J. Xie et al., "Study on relationship between density and mechanical behavior of high polymer grouting materials," *Journal of Wuhan University of Technology*, vol. 36, no. 4, pp. 44–47, 2014.

[18] J.-P. Balayssac and V. Garnier, *Non-destructive Testing and Evaluation of Civil Engineering Structures*, Elsevier, 2017.

[19] K. Schabowicz, "Non-destructive testing of materials in civil engineering," *Materials*, vol. 12, no. 19, p. 3237, 2019.

[20] I. Beverte, S. Gaidukovs, J. Andersons, and V. Skruls, "The impact of atmospheric parameters on the dielectric permittivity values of SikaBlock®-M150 and other rigid polyurethane foams measured with a capacitive one-side access sensor," *Sensors*, vol. 22, no. 20, p. 7859, 2022.

[21] I. Beverte, U. Cabulis, and S. Gaidukovs, "Polytetrafluoroethylene films in rigid polyurethane foams' dielectric permittivity measurements with a one-side access capacitive sensor," *Polymers*, vol. 13, no. 7, p. 1173, 2021.

[22] I. L. Al-Qadi, S. Lahouar, and A. Loulizi, "In situ measurements of hot-mix asphalt dielectric properties," *NDT & E International*, vol. 34, no. 6, pp. 427–434, 2001.

[23] S. Kim, J. Kang, S. H. Lee, and Y. H. Ahn, "Effect of chlorides on conductivity and dielectric constant in hardened cement mortar: NDT for durability evaluation," *Advances in Materials Science and Engineering*, vol. 2016, Article ID 6018476, 9 pages, 2016.

[24] F. Chen, N. Taylor, N. Kringos, and B. Birgisson, "A study on dielectric response of bitumen in the low-frequency range,"

Road Materials and Pavement Design, vol. 16, pp. 153–169, 2015.

[25] X. Yu, R. Luo, T. Huang, J. Wang, and Y. Chen, "Dielectric properties of asphalt pavement materials based on the temperature field," *Construction and Building Materials*, vol. 303, article 124409, 2021.

[26] X. H. Yu, R. Luo, J. T. Wang, and B. Wang, "Influence of relative humidity on the dielectric properties of asphalt mixture," *Journal of Huazhong University of Science and Technology (Natural Science Edition)*, vol. 49, no. 1, pp. 106–109, 2021.

[27] X. H. Yu, R. Luo, J. T. Wang, C. Li, and Y. Su, "Development of temperature–frequency equivalence principle on asphalt mixtures," *Journal of Central South University (Science and Technology)*, vol. 52, no. 7, pp. 2268–2275, 2021.

[28] H. Liu, F. Wang, M. Shi, and W. Tian, "Mechanical behavior of polyurethane polymer materials under triaxial cyclic loading: a particle flow code approach," *Journal of Wuhan University of Technology-Mater. Sci. Ed.*, vol. 33, no. 4, pp. 980–986, 2018.

[29] M. S. Shi, *Research on Polymer Grouting Material Properties and Directional Fracturing Grouting Mechanism for Dykes and Dams*, Dalian University of Technology, Dalian, 2011.

[30] M. Kirpluks, U. Cabulis, M. Kurańska, and A. Prociak, "Three different approaches for polyol synthesis from rapeseed oil," *Key Engineering Materials*, vol. 559, pp. 69–74, 2013.

[31] J. Wang, X. Li, H. Fang, J. Zhang, and J. Li, "Statistical characteristics of polymer grouting material microstructure," *Advances in Civil Engineering*, vol. 2020, Article ID 8847494, 12 pages, 2020.

[32] M. Hao, F. Wang, X. Li, B. Zhang, and Y. Zhong, "Numerical and experimental studies of diffusion law of grouting with expansible polymer," *Journal of Materials in Civil Engineering*, vol. 30, no. 2, p. 04017290, 2018.

[33] S. Pérez-Tamarit, E. Solórzano, A. Hilger, I. Manke, and M. A. Rodríguez-Pérez, "Multi-scale tomographic analysis of polymeric foams: a detailed study of the cellular structure," *European Polymer Journal*, vol. 109, pp. 169–178, 2018.

[34] U. Cabulis, I. Sevastyanova, J. Andersons, and I. Beverte, "Rapeseed oil-based rigid polyisocyanurate foams modified with nanoparticles of various type," *Polimery*, vol. 59, no. 3, pp. 207–212, 2014.

[35] GB/T 6343-2009, *Cellular Plastics and Rubbers-Determination of Apparent Density*, Standards Press of China, China, 2009.

[36] GB/T 12811-1991, *Test Method for Average Cell Size of Rigid Cellular Plastics*, Standards Press of China, China, 1991.

[37] Keysight Technologies, "N1501A Dielectric Probe Kit 10 MHz to 50 GHz," May 2020, https://www.keysight.com/us/en/assets/7018-04631/technical-overviews/5992-0264.pdf.

[38] J. H. Xu, M. Y. Shao, X. B. Li, and L. Lei, "Dielectric measurement method of soil moisture content based on quasi-static coaxial probe model," *Transactions of the Chinese Society for Agricultural Machinery*, vol. 52, no. 11, pp. 271–277, 2021.

[39] M. L. Meng, *Study on Dielectric Model Including the Frequency and Temperature of Concrete and Asphalt Mixture*, Zhengzhou University, Zhengzhou, 2014.

[40] A. Sihvola, "Electromagnetic Mixing Formulae and Applications. Number 47," in *IEE Electromagnetic Waves Series*, INSPEC, Inc., 2000.

[41] R. E. Newnham, D. P. Skinner, and L. E. Cross, "Connectivity and piezoelectric-pyroelectric composites," *Materials Research Bulletin*, vol. 13, no. 5, pp. 525–536, 1978.

[42] I. Beverte, V. Shtrauss, A. Kalpinsh et al., "Dielectric permittivity of rigid rapeseed oil polyol polyurethane biofoams and petrochemical foams at low frequencies," *Journal of Renewable Materials*, vol. 8, no. 9, pp. 1151–1170, 2020.

[43] G. Brodie, V. J. Mohan, and P. Farrell, "7 Dielectric Properties of Organic Materials," in *Microwave and Radio-Frequency Technologies in Agriculture: An Introduction for Agriculturalists and Engineers*, pp. 78–99, De Gruyter Open Poland, Warsaw, Poland, 2015.